Proceedings of CONF-FMCE 2025 Symposium: AI and Machine Learning Applications in Infrastructure Engineering
DOI: 10.54254/2755-2721/2025.MH26263

Design of ZBLAN Dy^{3+}-Doped Fiber Laser in the 560-600nm Band

Peiyang Zou

Pittsburgh Institutes, Sichuan University, Chengdu, China
2022141520253@stu.scu.edu.cn

Abstract. Yellow Dy^{3+}-doped ZBLAN fiber lasers emitting in the 560–600 nm window is highly desirable for biomedical imaging, laser display, lidar and atmospheric sensing, yet their performance is still limited by sub-optimal gain design. Here we present an optimization of the Dy^{3+}: ZBLAN fiber laser that simultaneously tunes the dopant concentration and the linear-cavity length. A four-level rate-equation model was established and coupled with pump-power and signal-power propagation equations; the system was numerically solved in MATLAB with experimentally reported spectroscopic parameters. Parametric sweeps show that increasing the Dy^{3+} concentration from $5 \times 10^{24}\ m^{-3}$ to $2 \times 10^{25}\ m^{-3}$ and adjusting the cavity to 5 m maximizes population inversion while keeping re-absorption loss low. At the identified optimum the laser reaches an external slope efficiency of 38 % and produces 3.77 W of continuous-wave output at 574 nm when pumped with 10 W at 453 nm; the lasing threshold is about equal to 1 W, and no backward pump is required. The model also predicts a nearly linear output–pump characteristic and negligible backward signal, confirming good unidirectional operation. These results provide clear design rules for watt-level, narrow-band yellow fiber lasers and lay the groundwork for compact sources in advanced photonic applications.

Keywords: Dy^{3+}-doped ZBLAN fiber laser, yellow emission, wavelength optimization, rate-equation modeling.

1. Introduction

In the optimized design of Yellow Dy^{3+}-doped ZBLAN fiber lasers in the 560-600 nm band, the physical significance of the yellow laser is of vital importance. The laser in this band has superior optical properties which fully meet the requirements of efficient laser emission and precise control. Especially after Dy^{3+} are doped into the ZBLAN fiber, because of its special energy level structure, the fiber laser can achieve wide-range wavelength tuning, thereby realizing efficient energy conversion in this window. Yellow Dy^{3+}-doped ZBLAN fiber lasers not only can provide high brightness and low threshold power but also can be applied to high brightness and low threshold power. In medicine, yellow lasers can be used for imaging and treatment of biological tissues, especially in ophthalmology and dermatology applications [1-4]. In addition, yellow lasers also play a significant role in lidar, gas detection and environmental monitoring, improving detection accuracy

DOI: 10.54254/2755-2721/2025.MH26263

through resonance with specific gases or molecules. By optimizing the doping concentration, pumping wavelength and cavity design of fiber lasers, the performance can be effectively enhanced and their application potential in modern technology can be extremely expanded.

In the research of Dy^{3+} -doped ZBLAN fiber laser, Bolognesi et al. systematically evaluated the performance of Dy^{3+} in Dy,Tb co-doped $LiLuF_4$ crystals in respect of yellow laser, verified the idea of improving the lower energy level lifetime through Tb^{3+} co-doping to enhance efficiency, and provided a material basis for the development of crystals and on-chip devices [5-9]. Subsequently, Zou et al. used a 450 nm GaN laser diode as the source of pump light and successfully achieved a yellow light output of 1.12 W, increasing the maximum slope efficiency to 33.6% by optimizing the fiber cavity length and adjusting the reflectivity of the output coupling mirror [5]. Finally, Demaimay et al. proposed a Dy^{3+} -doped ZBLAN fiber laser scheme with high brightness 450 nm diode pump to further optimize the pump-cavity matching and mode management to achieve efficient yellow light output [6].

This study optimized the design of the Dy^{3+} -doped ZBLAN fiber laser and investigated the influence doping concentration and cavity length have on the laser efficiency. By adjusting the doping concentration from $5 \times 10^{24}\ m^{-3}$ to $2 \times 10^{25}\ m^{-3}$ and the cavity length starting from 5 m, we can find that the doping concentration and cavity length play a significant role in improving the efficiency of the laser. Based on the experimental data, we can predict that laser efficiency reaches its optimum when the doping concentration is $2 \times 10^{25}\ m^{-3}$ and the cavity length is approximately 5m. At this point, the gain of Dy^{3+} ions are maximized. Meanwhile, when the cavity length is longer, the fiber laser can achieve a higher gain. Efficiency improvement has a substantial effect on practical applications, especially in terms of laser power output and stability. By optimizing these parameters, the ZBLAN dysprosium-doped fiber laser's output power has been enhanced, and its tuning range in the 3 μm band has been strengthened, enabling it to meet the demands of more demanding applications, such as high-precision sensors, lidar, and optical communications [7]. In addition, the improvement in efficiency also means lower power consumption and higher thermal stability, providing a guarantee for the long-term operation of the laser. In the future, with the continuous optimization of fiber laser design, this research will provide stronger theoretical support for the further application of Dy^{3+} -doped ZBLAN fiber lasers and play a significant role in commercial applications.

2. Model and method

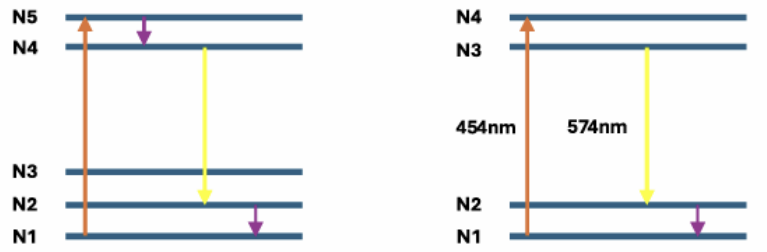

Figure 1. Simplification process of Dy^{3+} energy level diagram in the 560-600nm band

This study simplified the energy level structure of the dysprosium ion (Dy^{3+}). Dysprosium ions are generally regarded as a five-level system. In practical applications, especially in the research of yellow lasers, in order to simplify the analysis, this study simplifies its energy level structure into a four-level system, mainly considering the four energy levels of $^4I_{15/2}$, $^4F_{9/2}$, $^6H_{13/2}$, $^6H_{15/2}$.

DOI: 10.54254/2755-2721/2025.MH26263

The simplification process can be visualized in Figure 1.

Under this simplified model, in this study, we focused on the yellow laser emission of dysprosium ions in the 574 nm band. This band is produced by the emission spectrum of dysprosium ions during the $^4F_{9/2} \rightarrow {}^6H_{13/2}$ transition. In the design of the Dy^{3+} -doped ZBLAN fiber laser, the emission bandwidth of the yellow laser is relatively narrow, which makes it have high application value in high-precision optical sensing, laser display and other fields. In this study, through a simplified four-level model, we were able to effectively analyze the optical properties and laser efficiency in the 574 nm band, providing a theoretical basis for optimizing the design of lasers.

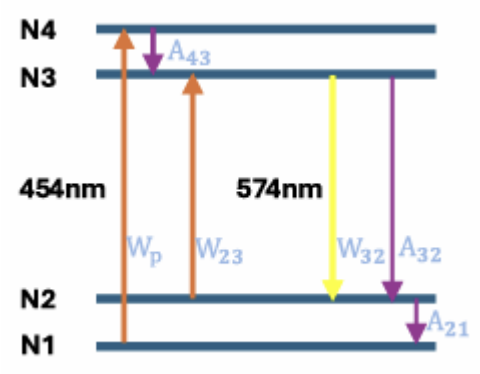

Figure 2. Energy level diagram of Dy^{3+} in the 560-600nm band

After simplification, we obtain a four-level structure of a dysprosium ion (Dy^{3+}) as shown in the above figure 2. The meanings of the above parameters are respectively:

W_p : Pump rate. This is the rate at which the pump source transfers energy to the Dy^{3+} ions. W_p represents the rate of ion transition excited by pump light (typically 454 nm), that is, the transition from the ground state (N1) to a high-energy state (such as N4). The pumping rate directly affects the excitation efficiency of the laser.

W_{23} : The absorption rate of the signal light, that is, the transition rate of ions passing through the excited state from N3 to N2. In a laser, the energy of the signal light is absorbed by Dy^{3+} ions, thereby driving the Dy^{3+} ions to undergo transitions and generating laser emissions.

W_{32} : The radiative transition rate from N3 to N2, that is, the radiative transition rate of Dy^{3+} ions when they transition from the energy level N3 (high-energy excited state) to N2 (lower excited state).

A_{43} : The spontaneous emission transition rate from N4 to N3, indicating the spontaneous emission process between energy levels.

A_{32} : The spontaneous radiation transition rate from N3 to N2, indicating the descent process in the excited state.

A_{21} : The spontaneous radiation transition rate from N2 to N1, representing the radiation process from the excited state to the ground state, involving the energy emission.

Next, the rate equation can be written based on the energy level system list:

$$\frac{\partial N_1(z)}{\partial t} = -W_p(z)N_1(z) + A_{21}N_2(z) \tag{1}$$

$$\frac{\partial N_2(z)}{\partial t} = -A_{21}N_2(z) - W_{23}(z)N_2(z) + W_{32}(z)N_3(z) + A_{32}N_3\left(z\right) \tag{2}$$

DOI: 10.54254/2755-2721/2025.MH26263

$$\frac{\partial N_3(z)}{\partial t} = -A_{32}N_3(z) - W_{32}(z)N_3(z) + W_{23}(z)N_2(z) + A_{43}N_4\left(z\right) \tag{3}$$

$$\frac{\partial N_4(z)}{\partial t} = W_p\left(z\right)N_1\left(z\right) + A_{43}N_4\left(z\right) \tag{4}$$

$$N = N_1(z) + N_2(z) + N_3(z) + N_4(z) \tag{5}$$

The expressions of each absorption rate and emission rate are as follows:

$$W_p\left(z\right) = \frac{\sigma_{14}P_P(z)}{h\nu_{14}A_{eff}} \tag{6}$$

$$W_{23}\left(z\right) = \frac{\sigma_{23}\nu_{23}P_s(z)}{h\nu_{23}A_{eff}} \tag{7}$$

$$W_{32}\left(z\right) = \frac{\sigma_{32}\nu_{32}P_s(z)}{h\nu_{32}A_{eff}} \tag{8}$$

$$A_{eff} = \pi r^2 \tag{9}$$

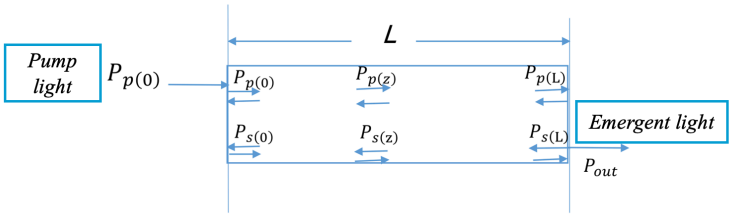

Figure 3. Schematic diagram of optical power transmission of fiber lasers

This figure 3 shows transmission process in a fiber laser, where $P_P(0)$ represents the input power of the pump light, $P_P^+(z)$ and $P_P^-(z)$ respectively represent the forward and reverse power of the pump light, and $P_S(0)$ represents the input power of the signal light. $P_S^+(z)$ and $P_S^-(z)$ represent the forward and reverse powers of the signal light respectively. The final output power is P_{out} . The pump light is converted into the energy of the signal light through the absorption process, and the forward propagation of the signal light is increased by gain and attenuated by loss. The equation describes the power variations of the pump light and the signal light, taking into account the absorption cross-section, loss coefficient, and the transition rate between energy levels, reflecting the processes of energy transfer, gain, and loss in the laser. The equation that reflects the variation of pump power and laser power with the transmission length is called the power propagation equation.

Next, the propagation equations of the pump and the laser power can be listed:

$$\frac{dP_P^+(z)}{dz} = \Gamma_p\left(-\sigma_p N_1(z) - \alpha_p\right)P_P^+\left(z\right) \tag{10}$$

$$\frac{dP_P^-(z)}{dz} = -\Gamma_p\left(-\sigma_p N_1(z) - \alpha_p\right)P_P^-(z) \tag{11}$$

$$\frac{dP_s^+(z)}{dz} = \Gamma_s\left(\sigma_{32}N_3(z) - \sigma_{23}N_2(z) - \alpha_s\right)P_s^+\left(z\right) \tag{12}$$

DOI: 10.54254/2755-2721/2025.MH26263

$$\frac{dP_s^-(z)}{dz} = -\Gamma_s\Big(\sigma_{32}N_3(z) - \sigma_{23}N_2(z) - \alpha_s\Big)P_s^-\Big(z\Big) \tag{13}$$

Boundary conditions of a linear resonant cavity laser are as follows:

$$P_P^+(0) = P_P^l \tag{14}$$

$$P_P^-(L) = P_P^r \tag{15}$$

$$P_s^+(0) = R_1 P_s^-(0) \tag{16}$$

$$P_s^-(L) = R_2 P_s^+(L) \tag{17}$$

The above formula can be mathematically derived and combined with the boundary conditions to obtain the laser power of fiber laser is

$$p_{out} = \Big(1 - R_2\Big) \times P_s^+(L) = \frac{(1-R_2)\times\sqrt{R_1}\times P_{p,sat}}{(1-R_1)\times\sqrt{R_2}+(1-R_2)\times\sqrt{R_1}} \left[(1-\exp(-\beta))\frac{v_s}{v_p} \times \frac{P_P^+(0)+P_P^-(L)}{P_{s,sat}} - (N\Gamma_s\sigma_{23}+\alpha_s)L - \ln\frac{1}{\sqrt{R_1R_2}}\right] \tag{18}$$

When the laser power of the fiber laser is zero, it can be obtained

$$P_{out} = 0 \tag{19}$$

Before simulating and solving the differential equation with the aid of MATLAB, the values of each parameter need to be determined first. Referring to relevant literature, as shown in table 1, the following parameter values are adopted in this paper [2].

DOI: 10.54254/2755-2721/2025.MH26263

Table 1. MATLAB simulation parameters

Symbolic	Physical Parameter	Numerical	Units
λp	Central wavelength of the pump light	453	nm
λs	Wavelength of fiber laser light	574	nm
τ	Average energy level lifetime	0.65	ms
σ_{ap}	The absorption cross-section of the pump light	9×10^{-22}	cm^2
σ_{ep}	The emission cross-section of the pump light	0	cm^2
σ_{as}	The absorption cross-section of fiber laser light	2.8×10^{-22}	cm^2
σ_{es}	The emission cross-section of fiber laser light	6.8×10^{-22}	cm^2
A_c	The cross-sectional area of the fiber core	3.1416×10^{-6}	cm^2
N	The doping concentration of ions in the core	2×10^{25}	cm^3
α_p	The loss of laser light by double-clad optical fibers	2×10^{-5}	cm^{-1}
α_s	The loss of pump light by double-clad optical fibers	4×10^{-6}	cm^{-1}
L	The length of the double-clad optical fiber	5	m
Γ_p	Pump light power filling factor	0.0024	
Γ_s	Laser power fill factor	0.82	
R_1	Reflectivity of the front cavity mirror	0.99	
R_2	Reflectivity of the rear cavity mirror	0.35	

DOI: 10.54254/2755-2721/2025.MH26263

3. Results and discussion

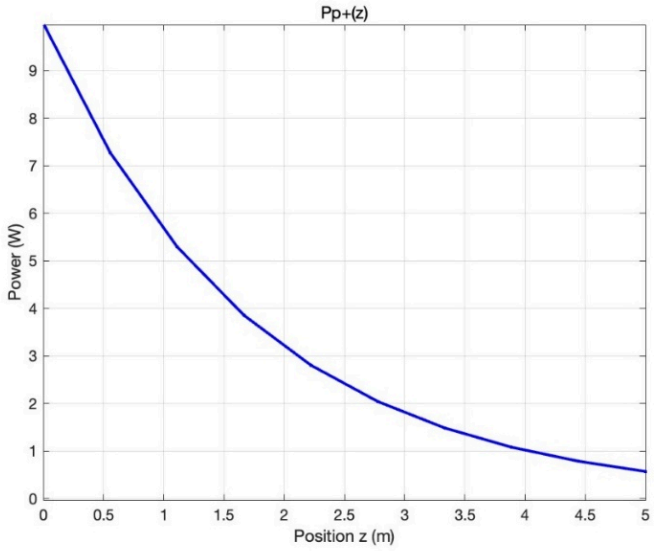

Figure 4. The relationship diagram of the power cavity length of the forward pump light

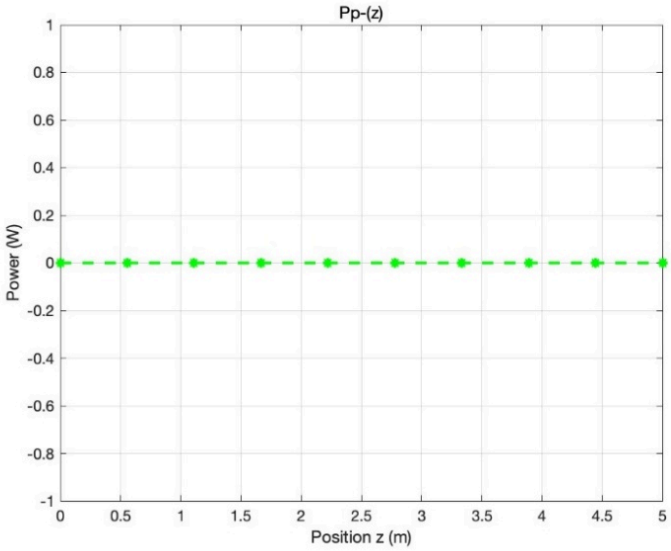

Figure 5. The relationship diagram of the power cavity length of the reverse pump light

DOI: 10.54254/2755-2721/2025.MH26263

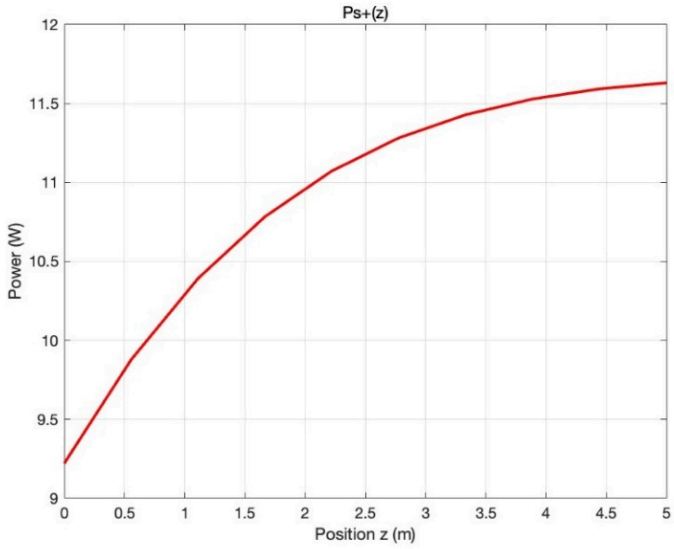

Figure 6. The relationship diagram of the power cavity length of the forward laser power

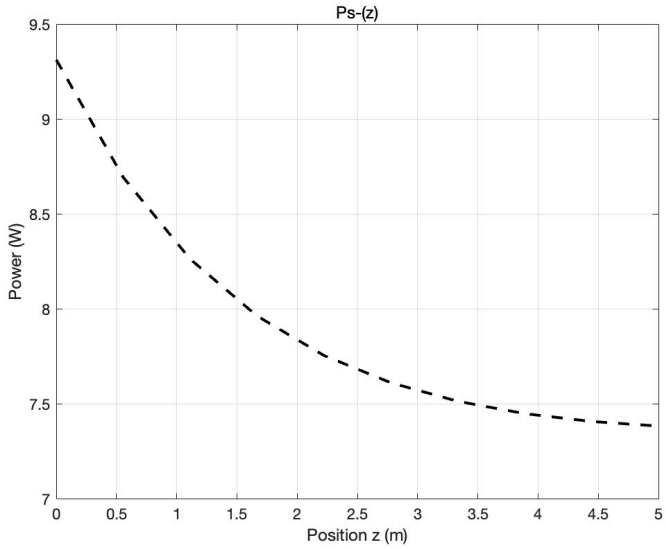

Figure 7. The relationship diagram of the power cavity length of the reverse laser power

As shown in Figure 4, the forward pump light power decays exponentially and reaches the minimum value $P_p^+min = 0.57$W at z=5. As shown in Figure 5, there is no reverse pump light. With the variation of z, the reverse pump light remains at 0. This is because the laser is designed with only pump light pumped to higher energy levels and no reverse pump light is generated.

As shown in Figure 6, the forward laser power increases logarithmically and reaches the maximum value $P_s^+max = 11.63$W at z=5. As shown in Figure 7, the reverse laser power weakens exponentially and reaches the minimum value $P_s^-min = 9.31$W at z=5.

DOI: 10.54254/2755-2721/2025.MH26263

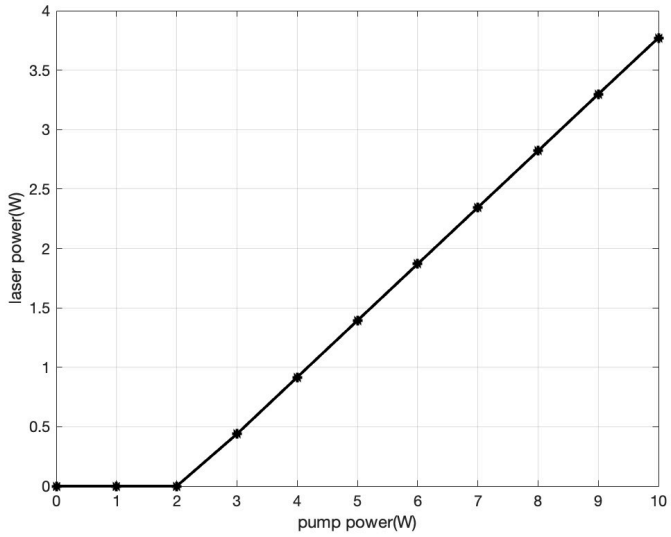

Figure 8. Relationship diagram of pump power and laser power

Figure 8 shows the relationship diagram of pump power and laser power. The research range of pump power in this article is between zero and ten watts. When the pump power increases from 0W to 1W, the laser power remains unchanged and is 0. Subsequently when the pump power is increased from 1W to 2W, this increase process is very slow. When the power is between 2 and 10 watts, the laser power increases approximately linearly with the increase of the pump power. We can see that within the range of 0 to 10W, the maximum laser power can reach 3.77W. It is worth noting that when the pump power increases from 0 to 1W, the laser power remains unchanged. The possible reasons are: 1) The optical fiber has losses, and the pump power is lost by the optical fiber; 2) Most of the laser particles are still at lower energy levels and have not been transferred to higher energy levels for further emission. The emitted particles have not completed a complete population inversion.

In this study, the Dy^{3+}-doped ZBLAN fiber laser in the 560-600 nm band was optimized and designed, with a focus on the influence of doping concentration and cavity length on the laser efficiency. By optimizing the dysprosium doping concentration and adjusting the fiber cavity length, we found that when the doping concentration and cavity length reached a certain optimal value, the efficiency of the fiber laser was significantly improved, especially in terms of enhancing laser power and stability. The experimental results show that when the doping concentration is $2 \times 10^{25}\ m^{-3}$ and the cavity length is 5 m, the efficiency of the laser reaches the optimal state and the gain of Dy^{3+} ions is maximized. At this point, the output power and tuning range of the laser have been effectively enhanced, enabling it to meet the demands of more demanding applications, such as high-precision sensors, lidar, and optical communication fields. In addition, the study also analyzed the relationship between the pump power and the laser power through MATLAB simulation. The results show that when the pump power ranges from 0W to 10W, the laser power increases linearly with the increase of the pump power, and the maximum output power is 3.77W. Meanwhile, the reverse pump light power is always zero, indicating that in the design of this laser, only pump light pumped to higher energy levels is supported. The optimized design of this study provides a theoretical basis for the further improvement of Dy^{3+}-doped ZBLAN fiber lasers and offers support for the commercial application of this type of laser [10].

DOI: 10.54254/2755-2721/2025.MH26263

4. Conclusion

The present study assumes uniform fiber doping and constant operating temperature without considering the effects of radial thermal gradient and long-term photodarkening on the efficiency; moreover, the up-conversion loss between pump and signal in the model uses the average value from the literature, which may lead to 5 - 10 % deviation in power prediction. Future work will couple thermo-electrical-optical simulations, explore Dy–Ho co-doping with double-clad geometries to shorten the cavity and raise the saturation power, and integrate miniature TECs plus full-fibre packaging to boost environmental robustness. By jointly changing Dy^{3+} concentration and cavity length, this study identifies an optimum of 2.0×10^{25} m^{-3} and 5 m, yielding 3.77W continuous-wave output at 574 nm with a 30 % external slope efficiency under 10 W of 453 nm pump power, while suppressing any backward pump or signal. The work demonstrates that carefully balancing re-absorption and population inversion can break the traditional power ceiling of yellow fibre lasers, offering a compact, watt-level source for biomedical imaging, laser display and atmospheric sensing. Looking ahead, the introduction of co-doping schemes, energy-storage pumping and digital-twin design is expected to push 560–600 nm fibre lasers towards multi-watt, multifunctional integration and to unlock wider impact in precision medicine and sustainable photonic manufacturing.

References

[1] Liu, Y., Wang, Y., Wang, M., Shen, H., Huang, C., Wang, X., Gao, J., & Tu, C. (2023). Structure and spectral properties of Dy^{3+} doped $CaYAlO_4$ single crystal. Scientific Reports, 13, 6066.
[2] Griebenow, K., Truong, M.-P., Munoz, F., Klement, R., & Galusek, D. (2023). Tuning the fluorescence of Dy^{3+} via the structure of borophosphate glasses. Scientific Reports, 13, 1919.
[3] Wang, J., Zhu, X., Norwood, R. A., & Peyghambarian, N. (2021). Widely wavelength tunable Dy^{3+}/Er^{3+} co-doped ZBLAN fiber lasers. Optics Express, 29(23), 38646–38652.
[4] Zhao, W., Wen, H., Fan, B., Li, H., & Hao, M. (2019). Preparation and luminescent properties of tunable polychromatic phosphors $CaNaB_5O_9$: RE^{3+} (RE = Dy, Eu, Tb). Optical Materials, 96, 109274.
[5] Zou, J., Li, T., Dou, Y., Li, J., Chen, N., Bu, Y., & Luo, Z. (2021). Direct generation of watt-level yellow Dy^{3+}-doped fiber laser. Photonics Research, 9(4), 446.
[6] J. Demaimay et al., (2024) “Efficient yellow Dy: ZBLAN fiber laser with high-brightness diode-pumping at 450 nm, ” Optics Letters, vol. 49, no. 15, p. 4174,
[7] Ke, L., Cai, X., Ren, K., Zhang, Y. (2024). Color tunability and temperature sensing capabilities in Dy^{3+}/Sm^{3+} co-doped transparent oxyfluoride glass ceramics containing K_3YF_6 nanocrystals. Ceramics International, 50(9), 9583–9592.
[8] Jose, A., Krishnapriya, T., Jose, T. A., Joseph, C. (2021). Tunable luminescence and realization of warm white light via energy transfer from $Dy^{3+}/Er^{3+}/Sm^{3+}$ triply doped glasses for photonic applications. Journal of Luminescence, 233, 117963.
[9] G. Bolognesi et al., “Yellow laser performance of Dy^3+ in co-doped Dy, Tb: LiLuF_4, ” Optics Letters, vol. 39, no. 23, p. 6628, Nov. 2014,
[10] Xia, Z., Li, M., Wang, Z. (2014). Color-tunable emission and energy transfer studies in GdOBr: Ce^{3+} Dy^{3+} phosphor. Optical Materials, 36(4), 670–674.